Rend. Lincei Mat. Appl. 28 (2017), 553–572
DOI 10.4171/RLM/776

Fluid Mechanics — *Singular behavior of a vortex layer in the zero thickness limit*, by Francesco Gargano, Marco Maria Luigi Sammartino and Vincenzo Sciacca, communicated on February 10, 2017.

This paper is dedicated to the memory of Professor Giuseppe Grioli.

Abstract. — The aim of this paper is to study the Euler dynamics of a 2D periodic layer of non uniform vorticity. We consider the zero thickness limit and we compare the Euler solution with the vortex sheet evolution predicted by the Birkhoff–Rott equation. The well known process of singularity formation in shape of the vortex sheet correlates with the appearance of several complex singularities in the Euler solution with the vortex layer datum. These singularities approach the real axis and are responsible for the roll-up process in the layer motion.

Key words: Vortex-sheet, Birkhoff–Rott equation, vortex layer, singularity tracking methods

Mathematics Subject Classification: 76B47, 76F10, 35A20, 35Q35

1. Introduction

Shear layer flows naturally arise in many oceanic and atmospheric processes. These layers can be represented by a thin transition region across which the velocity of the flow experiences a rapid variation which is related to a large amount of vorticity within the layer. If the thickness of the layer goes to zero, one obtains a vortex sheet curve across which the velocity field has a discontinuity in the component tangent to the curve, while the vorticity is a Dirac δ concentrated on the curve.

To prove that the vortex sheet motion is the zero-thickness limit of the dynamics of a shear layer is an important problem that has been tackled through different approaches, like formal asymptotics, see [47, 26], numerical methods [6], rigorous methods, see [45, 9, 8]. In particular, in [9], for a layer of uniform vorticity distributed between two analytic curves, and through the use of the abstract Cauchy–Kowalewski theorem, the authors proved convergence to the Birkhoff–Rott (BR) dynamics; a rigorous estimate of the error in terms of the thickness of the layer was in fact given.

One of the main issues related to the mathematical treatment of vortex sheet flows is the Kelvin–Helmholtz instability. This phenomenon leads to the ill-posedness of the BR equation in Sobolev norms [15, 27], and to the finite time formation of curvature singularity. For analytic initial data, local in time well-posedness of the BR equation was achieved in [58], while long time existence

was proven in [14] for a small perturbation of the flat sheet. We mention that the singularity formation had been predicted by the analysis of Moore, see [48, 49] and also [3], and by direct numerical simulations [39, 55, 24].

To continue vortex sheet motion beyond the singularity time of the BR solution invokes models including regularization components such as finite layer thickness [6, 13], surface tension [52, 35, 4], vortex blob regularization [42, 2, 5, 43], Euler-α model [34, 7, 13], viscosity effects [59, 26, 20, 56], or a more sophisticated notion of BR solution [61]. Usually all these models ensure convergence to the vortex-sheet solution before the singularity formation, and allow the continuation of the vortex-sheet solution after the singularity time. The post-singularity motion is characterized by typical phenomena like roll-up and spiral formation with trailing arms wrapping around the core of the sheet.

In this work we shall analyze the motion of a 2D periodic inviscid thin layer on which a non uniform vorticity is concentrated. In the zero thickness limit the layer reduces to the infinite array of periodic vortex sheets introduced in [13]. We shall show that the small disturbances of the equilibrium solution of the BR equation are linearly unstable, and have an exponential growth rate which is dependent on the distance between two consecutive sheets. This instability is the mechanism leading to the finite time singularity formation. By applying the singularity tracking methods, we shall analyze the singularity formation for a flat sheet with non uniform strength; the results will be compared with the singularity analysis of the Euler dynamics of the small-thickness layer motion. Although the Euler solution does not develops a real singularity, we shall see how the solution has complex singularities whose distance form the real domain is dependent on the initial thickness of the layer, and how the singularities are compatible with an eruptive behavior of the vorticity within the layer.

The rest of the paper is organized as follows: in Section 2 we shall introduce the infinite array of periodic vortex sheets and we shall prove how the equilibrium solution of the BR equation develops a Kelvin–Helmholtz instability (Subsection 2.1), eading to the singularity formation in finite time (Subsection 2.2). In Section 3 we shall analyse the motion of a 2D inviscid thin vortex layer of non uniform vorticity. We shall perform the 2D singularity analysis on the Euler solution in Subsections 3.2 and 3.3.

2. Singularity formation

The initial configuration we shall consider is the infinite array of vortex sheets, already presented in [13]; it consists of planar curves, periodic in the tangential direction x, and evenly distributed along the normal direction y: on these curves the vorticity is concentrated as delta-function.

Across each curve the velocity field experiences a jump in the component tangential to the curve, and the vorticity concentrated along the curves can be expressed at each time t as

$$\omega(\boldsymbol{x}, t) = \sum_{h \in \mathbb{Z}} \hat{\gamma}(p, t)\delta(\boldsymbol{x} - \boldsymbol{x}_h(p, t)),$$

where $\boldsymbol{x}(p,t) = (x(p,t), y(p,t))$, $\boldsymbol{x}_h(p,t) = (x(p,t), y(p,t) - hL_y)$ is the generic h-th vortex sheet curve, δ is the Dirac function, and L_y is the distance between two consecutive sheets. The variable p is a Lagrangian variable constant along particle paths. The relevant quantities are the true vortex strength $\hat{\gamma}(p,t)$, which is a measure of the jump of the velocity field across the curves, and the time independent vortex strength $\gamma(p) = \hat{\gamma}(p,t)|\partial_p \boldsymbol{x}_h(p,t)|$.

Assuming that L_x is the periodicity in the tangential direction, one has

$$x(p + kL_x, t) = kL_x + x(p,t), \quad y(p + kL_x, t) = y(p,t), \quad \gamma(p + kL_x) = \gamma(p),$$

for each $k \in \mathbb{Z}$.

The motion of the generic marker $\boldsymbol{x}(p,t)$ of a sheet (hereafter we shall omit the subscript h in $\boldsymbol{x}_h$) is governed by the BR equation, see [53, 44]:

$$\frac{\partial \boldsymbol{x}(p,t)}{\partial t} = \fint_{-L_x/2}^{L_x/2} \gamma(\tilde{p}) \boldsymbol{K}_{L_x,L_y}(\boldsymbol{x}(p,t) - \boldsymbol{x}(\tilde{p},t))) \, d\tilde{p}, \tag{2.1}$$

where the integral is intended in the principal value sense.

One can show, see [1, 13], that the kernel $\boldsymbol{K}_{L_x,L_y}$ in (2.1) has the following form:

$$\boldsymbol{K}_{L_x,L_y}(\boldsymbol{x}) = \Big(\frac{\partial \Psi_{L_x,L_y}}{\partial y}(x,y), -\frac{\partial \Psi_{L_x,L_y}}{\partial x}(x,y) \Big), \tag{2.2}$$

where

$$\Psi_{L_x,L_y}(x,y) = \frac{x^2}{2L_xL_y} - \frac{1}{2\pi} \log \left| \theta_1 \Big(\pi \Big(i\frac{x}{L_y} + \frac{y}{L_y} \Big), e^{-\pi \frac{L_x}{L_y}} \Big) \right|, \tag{2.3}$$

being $\theta_1(z,q) = 2\sum_{n=0}^{\infty} (-1)^n q^{(n+1/2)^2} \sin[(2n+1)z]$ the Jacobi theta function of the first kind.

The streamfunction (2.3) is the solution of the following periodic problem in the domain $\Omega = [-L_x/2, L_x/2] \times [-L_y/2, L_y/2]$, see [1]:

$$\begin{cases} \nabla^2 \Psi_{L_x,L_y}(x,y) = -\delta_{0,0}, \\ \Psi_{L_x,L_y}(-L_x/2, y) = \Psi_{L_x,L_y}(L_x/2, y), \quad \forall y \in [-L_y/2, L_y/2], \\ \Psi_{L_x,L_y}(x, -L_y/2) = \Psi_{L_x,L_y}(x, L_y/2), \quad \forall x \in [-L_x/2, L_x/2]. \end{cases} \tag{2.4}$$

One can therefore write explicitly the components of the kernel $\boldsymbol{K}_{L_x,L_y}$ as follows:

$$\begin{aligned} \boldsymbol{K}_{L_x,L_y}(\boldsymbol{x}) = \Bigg(& -\frac{1}{2L_y} \Re \left[\frac{\theta_1' \big(\pi \big(i\frac{x}{L_y} + \frac{y}{L_y} \big), e^{-\pi \frac{L_x}{L_y}} \big)}{\theta_1 \big(\pi \big(i\frac{x}{L_y} + \frac{y}{L_y} \big), e^{-\pi \frac{L_x}{L_y}} \big)} \right], \\ & - \frac{x}{L_xL_y} - \frac{1}{2L_y} \Im \left[\frac{\theta_1' \big(\pi \big(i\frac{x}{L_y} + \frac{y}{L_y} \big), e^{-\pi \frac{L_x}{L_y}} \big)}{\theta_1 \big(\pi \big(i\frac{x}{L_y} + \frac{y}{L_y} \big), e^{-\pi \frac{L_x}{L_y}} \big)} \right] \Bigg). \end{aligned} \tag{2.5}$$

2.1. The Kelvin–Helmholtz instability

In this Subsection we shall explain how, for the infinite array of periodic vortex sheet configuration, the BR equation develops the Kelvin–Helmholtz instability.

We first write the BR equation (2.1) in terms of the complex variable $z(p,t) = x(p,t) + iy(p,t)$ as

$$\frac{\partial z^*(p,t)}{\partial t} = \fint_{-L_x/2}^{L_x/2} \gamma(\tilde{p})[\mathcal{K}_S(z(p,t) - z(\tilde{p},t)) + \mathcal{K}_x(z(p,t) - z(\tilde{p},t))]\, d\tilde{p} \tag{2.6}$$

where z^* denotes the complex conjugate of z, and the kernels $\mathcal{K}_S$, $\mathcal{K}_x$ are defined as

$$\mathcal{K}_S(z) = -\frac{1}{2L_y} \frac{\theta_1'\left(\pi \frac{\tilde{z}(p,t) - \tilde{z}(\tilde{p},t)}{L_y}, e^{-\pi \frac{L_x}{L_y}}\right)}{\theta_1\left(\pi \frac{\tilde{z}(p,t) - \tilde{z}(\tilde{p},t)}{L_y}, e^{-\pi \frac{L_x}{L_y}}\right)}, \quad \tilde{z} = -iz, \tag{2.7}$$

$$\mathcal{K}_x(z) = \frac{i}{2L_xL_y}(z + z^*). \tag{2.8}$$

From the properties of the θ_1 function we have

$$\mathcal{K}_S^*(z) = \mathcal{K}_S(z^*).$$

To show how the Kelvin–Helmholtz instability forms, we determine the growth rate of the perturbation of an equilibrium solution of (2.6). It is easy to check that the flat solution $z_h(p,t) = z(p,t) + ihL_y = p + ihL_y$, $\gamma(p) = 1$ is an equilibrium solution for the BR equation. We now consider the linear evolution of $z_h(p) = p + ihL_y + \mu(p,t)$ where $\mu(p,t) = A_{\tilde{k}}(t)e^{i\tilde{k}p} + B_{\tilde{k}}(t)e^{-i\tilde{k}p}$, being $|A_{\tilde{k}}(0)| \ll 1$, $|B_{\tilde{k}}(0)| \ll 1$; $\tilde{k} = 2\pi k/L_x$ where $k \in \mathbb{Z}$.

To write the equation for the time evolution of the disturbance μ first we use

$$\sum_{k,h\in\mathbb{Z}} \frac{1}{z - \pi(h + ik\lambda)} = \frac{\theta_1'(z, e^{-\pi\lambda})}{\theta_1(z, e^{-\pi\lambda})},$$

where $\theta_1'(z,q)$ denotes the derivative with respect to z of θ_1; second the periodicity condition

$$z_h(p + kL_x, t) = z_0(p,t) + kL_x + ihL_y, \quad \forall k, h \in \mathbb{Z},$$

obtaining that

$$
\begin{aligned}
&\fint_{-L_x/2}^{L_x/2} \gamma(\tilde{p})[\mathcal{K}_S(z(p,t)-z(\tilde{p},t))]\,d\tilde{p} \\
&\quad = -\frac{1}{2\pi}\sum_{k,h\in\mathbb{Z}} \fint_{-L_x/2}^{L_x/2} \frac{\gamma(\tilde{p})}{\tilde{z}(p,t)-\tilde{z}(\tilde{p},t)-ikL_x-hL_y}\,d\tilde{p} \\
&\quad = -\frac{1}{2\pi}\sum_{k,h\in\mathbb{Z}} \fint_{(k-1/2)L_x}^{(k+1/2)L_x} \frac{\gamma(\tilde{p})}{\tilde{z}(p,t)-\tilde{z}_h(\tilde{p}-kL_x,t)}\,d\tilde{p} \\
&\quad = -\frac{1}{2\pi}\sum_{h\in\mathbb{Z}} \fint_{\infty}^{-\infty} \frac{\gamma(\tilde{p})}{\tilde{z}(p,t)-\tilde{z}_h(\tilde{p},t)}\,d\tilde{p}.
\end{aligned}
$$

Hence, the equation of the perturbation μ has the following form:

$$
\begin{aligned}
\frac{\partial\mu(p,t)^*}{\partial t} &= \frac{1}{2\pi i}\sum_{h\in\mathbb{Z}} \fint_{-\infty}^{\infty} \frac{1}{p-\tilde{p}+ihL_y+(\mu(p,t)-\mu(\tilde{p},t))}\,d\tilde{p} \\
&\quad + \frac{i}{2L_y}(\mu(p,t)+\mu^*(p,t))
\end{aligned}
\tag{2.9}
$$

and, as $(\mu(p,t)-\mu(\tilde{p},t))$ is small, to leading order we obtain

$$
\begin{aligned}
\frac{\partial\mu(p,t)^*}{\partial t} &= \frac{1}{2\pi i}\sum_{h\in\mathbb{Z}} \Big(\fint_{-\infty}^{\infty} \frac{1}{p-\tilde{p}+ihL_y}\,d\tilde{p} - \fint_{-\infty}^{\infty} \frac{(\mu(p,t)-\mu(\tilde{p},t))}{(p-\tilde{p}+ihL_y)^2}\,d\tilde{p} \Big) \\
&\quad + \frac{i}{2L_y}(\mu(p,t)+\mu^*(p,t)).
\end{aligned}
\tag{2.10}
$$

The first integral (2.10) vanishes, and by means of integrating by parts the second integral we obtain

$$
\begin{aligned}
\frac{\partial\mu(p,t)^*}{\partial t} &= -\frac{1}{\pi i}\hat{\sum_{h=0}^{+\infty}} \fint_{-\infty}^{\infty} \frac{\mu_p(\tilde{p},t)(p-\tilde{p})}{(p-\tilde{p})^2+(hL_y)^2}\,d\tilde{p} \\
&\quad + \frac{i}{2L_y}(\mu(p,t)+\mu^*(p,t)).
\end{aligned}
\tag{2.11}
$$

where $\mu_p = \partial_p\mu$, and the symbol $\hat{\sum}$ means that the term for $h=0$ is multiplied by a factor 1/2.

As

$$
\fint_{-\infty}^{+\infty} \frac{e^{\pm i\tilde{k}\tilde{p}}(p-\tilde{p})}{(p-\tilde{p})^2+(hL_y)^2}\,d\tilde{p} = \mp i\pi e^{-\tilde{k}hL_y\pm i\tilde{k}p}
$$

and substituting in (2.11) we obtain

$$\begin{aligned}(2.12)\quad \dot{A}^*_{\tilde{k}}(t)e^{-i\tilde{k}p}+\dot{B}^*_{\tilde{k}}(t)e^{i\tilde{k}p} &= i\tilde{k}\hat{\sum}_{h=0}^{+\infty}[A_{\tilde{k}}(t)e^{-\tilde{k}hL_y+i\tilde{k}p}+B_{\tilde{k}}(t)e^{-\tilde{k}hL_y-i\tilde{k}p}]\\ &\quad+\frac{i}{2L_y}(A_{\tilde{k}}e^{i\tilde{k}p}+B_{\tilde{k}}e^{-i\tilde{k}p}+A^*_{\tilde{k}}e^{-i\tilde{k}p}+B^*_{\tilde{k}}e^{i\tilde{k}p})\\ &=\frac{i\tilde{k}(e^{\tilde{k}L_y}+1)}{2(e^{\tilde{k}L_y}-1)}[A_{\tilde{k}}(t)e^{i\tilde{k}p}+B_{\tilde{k}}(t)e^{-i\tilde{k}p}]\\ &\quad+\frac{i}{2L_y}(A_{\tilde{k}}e^{i\tilde{k}p}+B_{\tilde{k}}e^{-i\tilde{k}p}+A^*_{\tilde{k}}e^{-i\tilde{k}p}+B^*_{\tilde{k}}e^{i\tilde{k}p}),\end{aligned}$$

where we have used $\sum_{h=0}^{+\infty}e^{-hx}=e^x/(e^x-1)$ for $x>0$. From (2.12) we obtain the following system of ODE

$$(2.13)\qquad \dot{Z}(t)=\mathscr{A}Z(t),$$

where $Z(t)=(\Re(A_{\tilde{k}}(t)),\Im(A_{\tilde{k}}(t)),\Re(B_{\tilde{k}}(t)),\Im(B_{\tilde{k}}(t)))$, and

$$\mathscr{A}=\begin{pmatrix}0 & \frac{1}{2L_y} & 0 & q\\ -\frac{1}{2L_y} & 0 & q & 0\\ 0 & q & 0 & \frac{1}{2L_y}\\ q & 0 & -\frac{1}{2L_y} & 0\end{pmatrix},$$

where $q=-\frac{\tilde{k}(e^{\tilde{k}L_y}+1)}{2(e^{\tilde{k}L_y}-1)}-\frac{1}{2L_y}$. The matrix $\mathscr{A}$ admits a positive eigenvalue with multiplicity 2

$$\lambda=\sqrt{\frac{\tilde{k}^2(e^{\tilde{k}L_y}+1)^2}{4(e^{\tilde{k}L_y}-1)^2}+\frac{(e^{\tilde{k}L_y}+1)}{2L_y(e^{\tilde{k}L_y}-1)}}.$$

Therefore the linearized modes of any disturbances have positive growth rate, implying an ill-posed linear motion. This is known as the Kelvin–Helmholtz instability. We notice that if we let $L_y\to\infty$, and take $L_x=2\pi$, the infinite array of periodic vortex sheets reduces to the classical single periodic vortex sheet curve, see [39, 55]. In this case $\lambda=k/2$ which is exactly the growth rate reported in [39, 55] for the periodic vortex sheet.

2.2. *Singularity formation for the Birkhoff–Rott solution*

In this section we show how the Kelvin–Helmholtz instability induces the singularity formation in finite time for the solution of the BR equation.

For the purpose of our analysis we need to compute the numerical solution of (2.1). In particular we use a fourth order Runge–Kutta scheme as temporal

discretization and, following Krasny [39], we compute the numerical value of the integral in (2.1) by using the alternating point quadrature formula. To evaluate the θ_1 function it is enough to consider in the summation only the first 20 terms, because the summation rapidly decreases to zero with n. The main difficulty in computing the vortex sheet motion is related to the Kelvin–Helmholtz growth of the round-off disturbances. To avoid this unwanted phenomenon, we apply the filtering technique proposed by Krasny in [39], according to which at each time step the Fourier modes having amplitude smaller than the threshold value 10^{-27} are set to zero. Computation is performed with 32-digit precision.

We consider, as initial condition, the flat sheets with a sinusoidal vortex strength

$$\boldsymbol{x}(p,0) = (p,0), \quad \gamma(p) = \sin(p), \quad p \in [-\pi, \pi], \tag{2.14}$$

and $L_x = L_y = 2\pi$.

To analyze the process of the singularity formation we apply the singularity tracking method, which allows to determine the position and the algebraic character of the complex singularity nearest to the real axis. This method has been widely used to perform a singularity analysis in equations arising in fluid dynamics. Besides the paper cited in the introduction for the BR equation, we recall here the applications to the incompressible Euler flow, see [10, 28, 46, 21, 51], to boundary layer flow, see [23, 25, 30, 31, 32, 33], to Camassa–Holm and Degasperi–Procesi equations, [25, 22], to the KdV equation in [36, 29], and others [36, 37, 38, 60]. See also the recent review paper [11] on the various singularity tracking procedures.

The complex singularity tracking method is based on the link between the asymptotic properties of the Fourier spectrum and the radius of analyticity of a real function. In particular, suppose that $u(z)$ is a real function having a complex singularity in $z^* = x^* + i\delta^*$ and that $u(z) \approx (z - z^*)^{\alpha + i\tau}$, using a steepest descent argument it is possible to give the asymptotic (in k) behaviour of the spectrum u_k of $u(z)$:

$$u_k \approx C_X k^{-(\alpha+1)} e^{-\delta^* k} \sin(kx^* + \tau \log(k) + \phi). \tag{2.15}$$

To apply the singularity tracking method to BR solution, we consider the Fourier modes of the components

$$(X(p,t), Y(p,t)) = \boldsymbol{x}(p,t) - p = \Big(\sum_k X_k(t) e^{ikp}, \sum_k Y_k(t) e^{ikp} \Big),$$

obtained from the numerical solution of (2.1). Hence, the asymptotic behaviour of the spectrum of X for large k (same arguments for the component Y and its Fourier modes) is:

$$X_k(t) \approx C_X(t) k^{-(\alpha_X(t)+1)} e^{-\delta_X(t) k} \sin(k\xi_X(t) + \tau_X(t) \log(k) + \phi_X(t)), \tag{2.16}$$

where $z^* = \xi_X + i\delta_X$ is the position of the singularity. The best way to find the parameters C_X, α_X, δ_X, ξ_X, τ_X, ϕ_X in (2.16) is to perform a fitting procedure to the logarithmic of (2.16). In particular, we suppose that (2.16) holds point-wise for each k, and equating six consecutive modes $X_{k-5}, \ldots, X_k$ to the form in (2.16) we obtain a system for the parameters C_X, α_X, δ_X, ξ_X, τ_X, ϕ_X whose solution returns the k-dependent values of the parameters. The values of the various parameters are actually retrieved in the band of k where they are almost k-independent, and this happens in general in the first 30–100 modes.

Results show that both components have a singularity in the same position in the complex plane (that is $\delta_X(t) \approx \delta_Y(t)$ and $\xi_X(t) \approx \xi_Y(t)$), while the two characterizations α_X and α_Y are different. The time evolutions of the width of the analyticity $\delta_X = \delta_Y$ is shown in Figure 1(a), while the time evolutions of the characterizations α_X, α_Y are shown in Figure 1(b). We have found that at $t_s \approx 1.911$ the singularity hits the real domain ($\delta_X = 0$) in $p^* \approx \pi/2$, and that the characterizations are $\alpha_X \approx 1.84$ and $\alpha_Y \approx 1.97$, being the values of τ_X, τ_Y of order 10^{-2} at t_s. Notice that for symmetry reasons there is also a singularity placed in $-p^*$. This means that both the components $(X(p,t), Y(p,t))$ experience at t_s a blow-up in their second derivative in p^* due to the presence of a branch singularity. As X and Y have a blow up in their second derivatives, the curve at time t_s has a smooth behavior as shown in Figure 2(a), while the eruptive behavior of the second derivatives can be deduced from Figure 2(b), where the time evolution of X_{pp} from $t = 1.7$ up to $t = 1.9$ (just prior the singularity time) is shown: in p^* the second derivative X_{pp} rapidly decreases for $p \to (p^*)^-$ while it rapidly increases for $p \to (p^*)^+$ (Y_{pp} has a similar behavior).

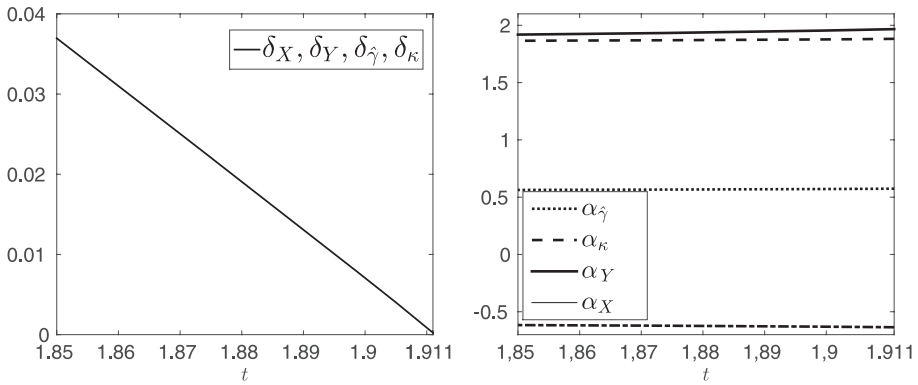

(a) (b)

Figure 1. a) The time evolutions of the width of the analyticity δ_X, δ_Y, δ_κ, $\delta_{\hat{\gamma}}$ of X, Y, κ, $\hat{\gamma}$ from $t = 1.85$ up to $t_s = 1.911$. At t_s $\delta_X = \delta_Y = \delta_\kappa = \delta_{\hat{\gamma}} \approx 0$ meaning that the BR solution develops a singularity. b) The time evolutions of the characterizations α_X, α_Y, α_κ, $\alpha_{\hat{\gamma}}$ from $t = 1.85$ up to $t_s = 1.911$. At t_s, $\alpha_X \approx 1.84$, $\alpha_Y \approx 1.97$, $\alpha_\kappa \approx -0.63$, $\alpha_{\hat{\gamma}} \approx 0.55$.

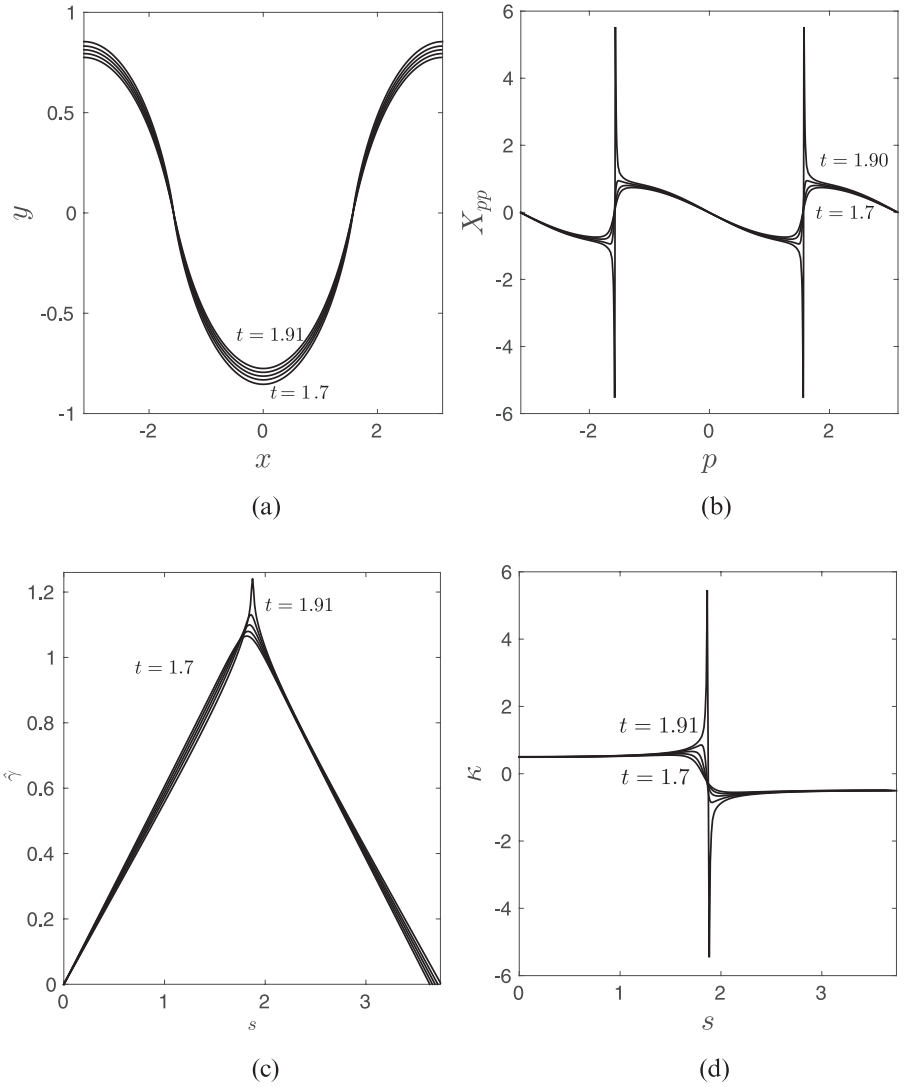

Figure 2. a) The vortex sheet curve from $t = 1.7$ up to $t = 1.9$ (time steps of 0.05) and $t = 1.91$, just prior the singularity time. b) Time evolution of the second derivative X_{pp} of the X component from $t = 1.7$ up to $t = 1.9$ (time steps of 0.05). At $t = 1.9$ the singularity is very close to the real domain, and X_{pp} exhibits an eruptive behavior in $p^* = \pm\pi/2$. c) Time evolution of the true vortex sheet strength $\hat{\gamma}$ in terms of the arc-length $s(p)$ from $p = 0$ (only $s \geq 0$ is shown). At $t = 1.91$ $\hat{\gamma}$ has a square-root cusp behavior in p^*. d) Time evolution of the curvature κ in terms of the arc length s (only $s \geq 0$ is shown). At $t = 1.91$ κ experiences an eruptive behaviour in p^*, similarly to the derivative X_{pp}.

At $t \approx t_s$ also the curvature $\kappa(p,t) = (x_p y_{pp} - y_p x_{pp})/((x_p^2 + y_p^2)^{3/2})$ and the true vortex sheet strength $\hat{\gamma}(p,t) = \gamma(p)/|x_p, y_p|$ become singular in p^*. Applying the singularity tracking method to k and $\hat{\gamma}$ we obtain that κ diverges, being the characterization $\alpha_\kappa \approx -0.63$, while $\hat{\gamma}$ forms a square-root cusp having characterization $\alpha_{\hat{\gamma}} \approx 0.55$ (see Figure 1(b)), and also in this case both the imaginary part of the complex characterizations due to the asymptotic behaviour in (2.16) is negligible. The time evolutions of the curvature κ and the true vortex sheet strength $\hat{\gamma}$ are shown in Figures 2(c), 2(d) from $t = 1.7$ up to $t = 1.91$ as functions of the signed arc length from $p = 0$.

3. Vortex layer of non uniform vorticity

In this Section we shall consider the regularization of the vortex sheet motion given by an inviscid layer of small thickness whose evolution is governed by Euler equations. Several authors considered this problem and compared the motion of a layer of uniform vorticity with the vortex sheet motion governed by the BR equation, see [48, 6, 9, 26]. Here we consider a layer of non uniform vorticity concentrated on the layer of thickness ε.

Following the analysis performed in [13], we introduce the rescaled variable $Y = y/\varepsilon$ and assume the initial vorticity to be of the form

$$\omega_0(x,y) = \varepsilon^{-1} f(x,Y), \tag{3.1}$$

where $f(x,Y)$ has a rapid decay in Y, and $\int f(x,Y)\,dY$ is finite. In the limit $\varepsilon \to 0$, the layer shrinks to a sheet.

The Euler equations in the vorticity-streamfunction formulation are the following:

$$\partial_t \omega + u\partial_x \omega + v\partial_y \omega = 0, \tag{3.2}$$

$$\partial^2_{xx}\psi + \partial^2_{yy}\psi = -\omega, \tag{3.3}$$

$$u = \partial_y \psi, \quad v = -\partial_x \psi, \tag{3.4}$$

$$\omega(x,y,t=0) = \varepsilon^{-1} f(x,Y), \tag{3.5}$$

$$f(x,Y) = \sin(x)\exp(-Y^2/2)/\sqrt{2\pi}. \tag{3.6}$$

The problem is solved in the periodic domain $D = [-\pi,\pi] \times [-\pi,\pi]$. Equation (3.2) is the vorticity-transport equation, (3.3) is the Poisson equation for the streamfunction, and equation (3.4) links the streamfunction to the velocity components. The initial condition is given by (3.5) and (3.6), and it represents a flat layer having thickness of order ε, in which the vorticity strength has a sinusoidal profile along the tangential direction, and it has a highly peaked gaussian profile along the normal direction. Numerical simulations are employed by using a fully spectral numerical scheme with a semi-implicit third order Runge–Kutta scheme as temporal discretization, see [62].

3.1. Vortex layer motion

We have performed several numerical simulations of (3.2)–(3.6) with the regularization parameter ranging from $\varepsilon^2 = 0.02$ up to $\varepsilon^2 = 0.005$. To compare the vortex layer motion with the vortex sheet dynamics, we consider the material curve $\mathscr{C}$ which, at $t = 0$, is placed in the center of the layer. We evolve in time the curve $\mathscr{C}$ following the lagrangian path of fluid particles initially distributed on $\mathscr{C}$.

The behavior of $\mathscr{C}$ is shown at time $t = 1.91$, just prior the singularity time of the BR solution, in Figure 3(a) for the various ε, and compared with the BR solution. As one could expect, the curve $\mathscr{C}$ shows a better agreement with the BR case as $\varepsilon \to 0$.

After the singularity time for the BR solution, the typical roll-up process of the thin vorticity layer begins to manifest (see also [59, 13] for the roll-up process of vorticity layer). For all the ε considered, the vorticity concentrates close to the points where the singularity should form in the vortex sheet governed by the BR equation (i.e. in $p = \pm\pi/2$) and, due to the incompressibility condition, the flow bulges outwards close to that points, leading to the formation of two cores of negative and positive vorticity visible for instances in Figures 3(b)–3(d) for $\varepsilon^2 = 0.02, 0.005$ at $t = 6$, and $\varepsilon^2 = 0.005$ at $t = 4$. As time passes the two cores begin to rotate in opposite direction, and two spirals with trailing arms wrapping around the cores of the layer form. In Figures 3(c), 3(e) the spirals are well visible for $\varepsilon^2 = 0.02, 0.005$ at $t = 6$.

The different initial thickness of the layer induces different flow motion. From Figures 3(b)–3(d) one can observe how the roll-up process is more sustained for the lower ε, with the curve $\mathscr{C}$ showing, at a specific time, an increasing number of windings for decreasing ε.

3.2. Singularity analysis

Although the vortex layer, and consequently the curve $\mathscr{C}$, is regular for all time, it is of interest to characterize the complex singularities of the layer solution, and how they are related to the parameter ε.

In order to perform the singularity analysis of Euler's solution, we apply the singularity tracking method for bi-variate function, see [46, 51] and also [30, 32, 33]. In particular, given the Fourier expansion of Euler's solution

$$\omega(x, y) = \sum_{k_1, k_2} \omega_{k_1 k_2} e^{ik_1 x} e^{ik_2 y},$$

if one considers those modes (k_1, k_2) such that $k_1 = k\cos\theta$ and $k_2 = k\sin\theta$, where $k = |(k_1, k_2)|$, then the Fourier coefficients, for $k \to \infty$, have the following asymptotic behavior:

$$\omega_{k_1 k_2} \approx k^{-(\alpha(\theta)+1)} e^{-\delta(\theta)k} e^{ikx^*(\theta)}, \quad \text{where } (k_1, k_2) = k(\cos\theta, \sin\theta). \tag{3.7}$$

The width of the analyticity strip δ^* is the minimum over all directions θ, i.e. $\delta^* = \min_\theta \delta(\theta)$.

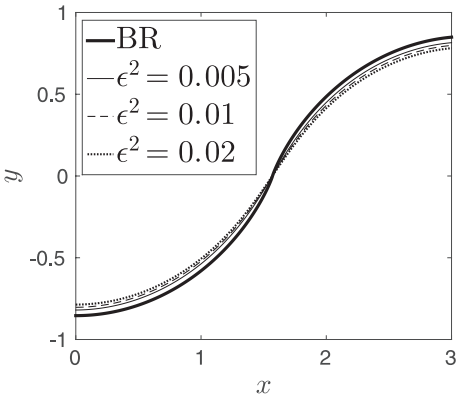

(a) $t = 1.91$

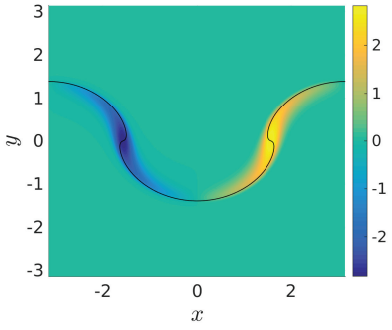

(b) $\epsilon^2 = 0.02, t = 4$

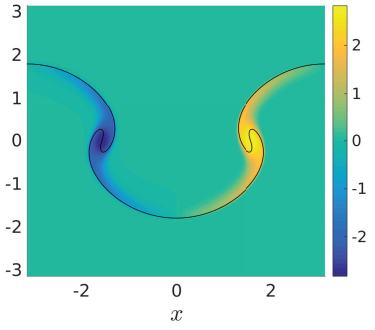

(c) $\epsilon^2 = 0.02, t = 6$

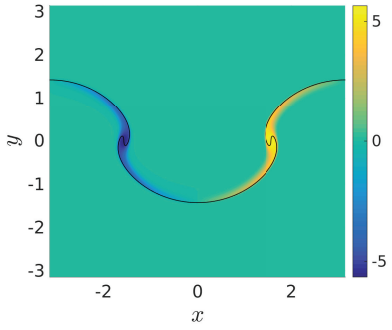

(d) $\epsilon^2 = 0.005, t = 4$

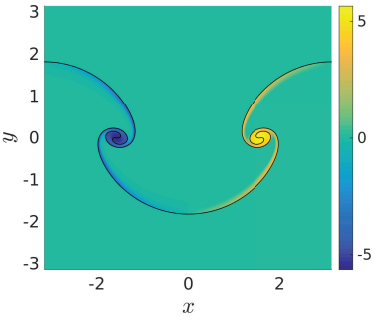

(e) $\epsilon^2 = 0.005, t = 6$

Figure 3. a) Vortex sheet curve for the BR equation and the material curves $\mathscr{C}$ for various values of the initial thickness of the layer at $t = 1.91$ (just prior the singularity formation for the BR solution). b)–c) Vorticity distribution for the vortex layer and material curve $\mathscr{C}$ (black lines) for $\varepsilon^2 = 0.02$ at $t = 4$ and $t = 6$. d)–e) Vorticity distribution for the vortex layer and material curve $\mathscr{C}$ (black lines) for $\varepsilon^2 = 0.005$ at $t = 4$ and $t = 6$.

When dealing with bi-variate function it is more convenient to work with the shell-summed Fourier amplitudes, defined as

$$A_K \equiv \sum_{K \le |(k_1,k_2)| < K+1} |\omega_{k_1 k_2}|. \tag{3.8}$$

The asymptotic behavior of these amplitudes is, see [51]

$$A_K \approx C K^{-(\alpha_{Sh}+1/2)} \exp(-\delta_{Sh} K) \quad \text{when } K \to \infty, \tag{3.9}$$

where δ_{Sh} gives the width of the analyticity strip and α_{Sh} gives information on the characterization of the singularity. As proven in [51], if one denotes with θ^* the angle where $\delta(\theta)$ takes its minimum (i.e. $\delta^* = \delta(\theta^*)$), then $\delta_{Sh} = \delta(\theta^*)$ and $\alpha_{Sh} = \alpha(\theta^*) - 1/2$, that is the rates of exponential and algebraic decay of the shell-summed Fourier amplitudes are, respectively, the width of the analyticity and the characterization of the most relevant complex singularity of the solution.

The shell-summed amplitudes of the vorticity ω of the Euler solution are shown in Figure 4(a) for various values of the initial thickness ε^2 at $t = t_s$ in lin-log scale. As expected, the amplitudes have decreasing exponential decay for decreasing ε (see Figure 4(b)). We also notice that the fitting procedures are in this case applied to particular bands of K. In fact, due to the initial choice the flat gaussian layer, the first part of the shell summed amplitudes exhibits for all ε almost a gaussian decay, so that it is convenient to focus only on the last range of the amplitudes which is actually affected by the presence of complex singularities. For instances for $\varepsilon^2 = 0.01$–0.02 only $K \ge 100$ are considered, whereas for $\varepsilon^2 = 0.005$ we considered $K \ge 200$ (see Figure 4(a)).

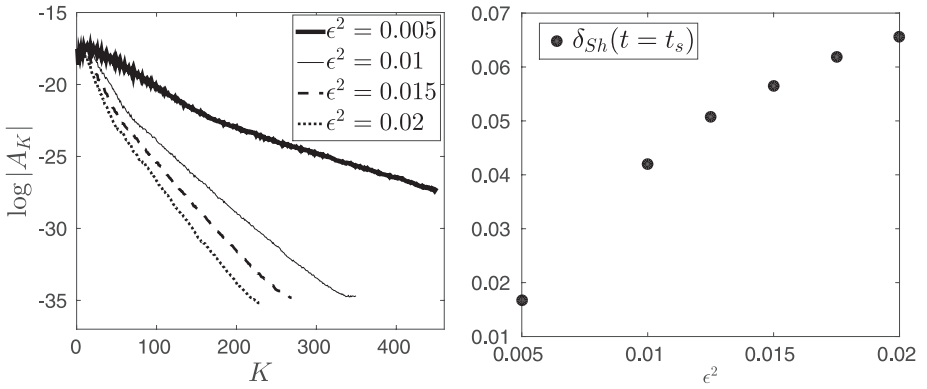

(a) (b)

Figure 4. a) Fourier shell summed amplitudes in lin-log scale at $t = t_s$ for various values of the initial thickness of the layer. For decreasing thickness the amplitudes exhibit a decreasing exponential decay rate, meaning that the width of the analyticity δ_{Sh} of the Euler solution decreases with ε. b) Width of the analyticity δ_{Sh} evaluated through (3.9) for various ε^2 at $t = t_s$.

Regarding the characterization of the singularity, which is obtained by determining the rate of algebraic decay α_{Sh} in (3.9), we have obtained that α_{Sh} is, at $t = 1.91$ of order $\alpha_{Sh} \approx -0.5$. This reveals that the vorticity has an inverse square root singularity, meaning that the complexified vorticity has an eruptive behaviour. This is somewhat expected, as the vorticity is highly concentrated and shows an eruptive behavior along the thin layer, especially for decreasing ε. The obtained characterization is also compatible with that found in [11] for the streamfunction of a viscous periodic thin layer of non uniform vorticity of distinguished sign. In particular in [11] it was shown that the streamfunction had a 3/2-characterized singularity, revealing an eruptive behavior in the second derivatives of the streamfunction and, consequently, in the vorticity. We stress here that the outcomes of the fitting procedures applied to (3.9) does not give any further information on all the possible complex singularities of the Euler solution. It is likely, in fact, that the various complex singularities actually form a complex manifold as predicted by previous analysis on the Euler equation with analytic initial data, [28, 46, 51].

3.3. Singularity analysis for the material curve $\mathscr{C}$

The aim of this subsection is to perform a comparison between the singularity of the BR solution, and the complex singularities of the curve $\mathscr{C}$ retrieved from the vortex layer motion presented in subsection 3.1. The analysis we shall present is different from the one presented in the previous subsection, as it is applied to the components of a curve, and it allows to retrieve information also on the position of the singularities.

We apply the singularity tracking methods, and in particular we use the Borel–Polya–van der Hoeven method (BPH). This method is very powerful, and it allows to retrieve information on the positions and the characterizations of the various algebraic singularities of an analytic function, extending the singularity tracking method based on the asymptotic behaviour (2.16). It was originally proposed in [50] to investigate on the various complex singularities of the Burgers equation, and later to analyse the complex singularities of a wall shear of a boundary layer flow ([32]), and the complex singularities for the regularized BR-α in [13]. We shall not give further details on this method, and we refer the interest reader to the previous cited papers for an exhaustive reading on this method and how can be applied.

Singularity tracking with the BPH method is applied to the Fourier expansion of the components $(X^\varepsilon(p,t), Y^\varepsilon(p,t)) = (x_{\mathscr{C}}(p,t) - p, y_{\mathscr{C}}(p,t))$, where $\mathscr{C} = (x_{\mathscr{C}}(p,t), y_{\mathscr{C}}(p,t))$. Up to t_s we have clearly distinguished and characterized, in both X^ε and Y^ε, two main complex singularities whose location will be denoted with $\tilde{p}_1^\varepsilon = p_{1,\varepsilon} + i\delta_{1,\varepsilon}$ and $\tilde{p}_2^\varepsilon = p_{2,\varepsilon} + i\delta_{2,\varepsilon}$[1]. In Figure 5(a), $\tilde{p}_1^\varepsilon$ and $\tilde{p}_2^\varepsilon$ are tracked in the complex plane at $t = 1.911$ and from $t = 2.5$ up to $t = 6$ (time steps of 0.5) for $\varepsilon^2 = 0.005, 0.01, 0.02$ (only $p \geq 0$ is shown). In the same figure the tracking of the BR singularity is shown from $t = 1$ up to $t = 1.91$. Due to the symmetry

[1] Hereafter we shall also label these singularities simply with their locations $\tilde{p}_1^\varepsilon$ and $\tilde{p}_2^\varepsilon$.

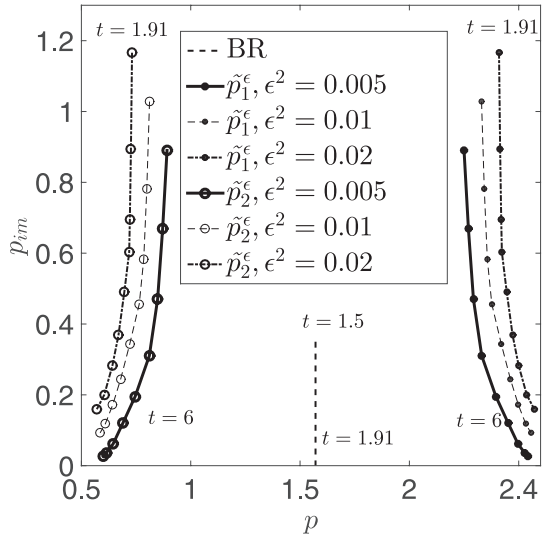

(a)

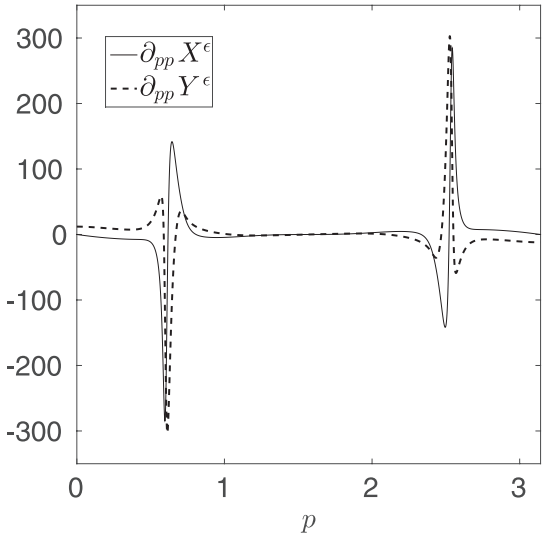

(b)

Figure 5. a) Tracking of the singularities $\tilde{p}_1^\varepsilon$, $\tilde{p}_2^\varepsilon$ in the complex p-plane at $t = 1.911$ and from $t = 2.5$ up to $t = 6$ (time steps of 0.5) for $\varepsilon^2 = 0.005, 0.01, 0.02$. The dashed line is the tracking of the BR singularity from $t = 1.5$ up to $t = 1.91$. All the singularities have characterizations compatible with the blow-up of the second derivatives of the components X^ε, Y^ε. b) Second derivatives $\partial_{pp} X^\varepsilon$, $\partial_{pp} Y^\varepsilon$ for $\varepsilon^2 = 0.005$ at $t = 6$. Both the derivatives have an eruptive behavior close to 0.61 and 2.52, very close to the real part of the singularities $\tilde{p}_1^\varepsilon$, $\tilde{p}_2^\varepsilon$.

of the problem, it is expected that the singularities $\tilde{p}_1^\varepsilon$ and $\tilde{p}_2^\varepsilon$ are symmetric with respect to π, and their distance from the real domain diminishes as time passes and for decreasing ε. Moreover as ε decreases the distance in the complex plane between the two singularities diminishes.

These singularities have similar characterizations for all times we have considered. In fact, we have determined through the BPH method that $\alpha^X_{\tilde{p}_1^\varepsilon} = \alpha^X_{\tilde{p}_2^\varepsilon}$ and $\alpha^Y_{\tilde{p}_1^\varepsilon} = \alpha^Y_{\tilde{p}_2^\varepsilon}$ have always values in the range (1.45–1.95) for all the time considered. The obtained characterizations are compatible with the BR-singularity, and reveal an eruptive behavior in the second derivative of the components X^ε and Y^ε. In Figure 5(b) $\partial_{pp}X^\varepsilon$, $\partial_{pp}Y^\varepsilon$ are shown for $\varepsilon = 0.005$ and $t = 6$, and they have an evident eruption close $p \approx 0.61$ and $p \approx 2.52$, very close to the real part of the positions of $\tilde{p}_1^\varepsilon$ and $\tilde{p}_2^\varepsilon$ (Figure 5(a)).

4. Conclusion

We have analyzed the motion of a vortex layer of non uniform vorticity whose evolution is governed by the Euler equation. The initial configuration we have studied, in the zero thickness limit, consists in an infinite array of periodic vortex sheets. The motion of the sheets is governed by the BR equation that, in finite time, develops a singularity. We have characterized, through the singularity tracking method, the singularities of the components of the curve as a 3/2 branch singularity. We have compared the vortex sheets motion with the dynamics of a material curve centered within the layer, and we have shown that, for small thickness of the layer, this material curve closely follows the BR solution. However due to the regularization induced by the finite thickness of the layer, this material curve does not develop singularity and, after the singularity time for the BR solution, shows well known features of the shear layer flow like roll-up process and spiral formation.

Although Euler solution is regular globally in time, we have shown through the singularity analysis that the solution has complex singularities whose distances from the real domain diminishes as the thickness of the layer goes to zero. Through the analysis of the Fourier shell summed amplitudes we have also characterized the relevant singularities, obtaining that the complex singularities are compatible with an eruptive behavior of the vorticity within the layer.

It remains still unsolved the question whether the various regularization of the BR equation have a common limit in the zero-regularization limits (vortex blob, Euler-α, approximation with viscous-inviscid layer), a problem that appears relevant also considering the non uniqueness results obtained in [43]. In [59] it was suggested that the blob methods well capture some large scale features of the viscous vortex-layer motion, and in [34] the authors numerically proved that blob and BR-α appear to be similar regularization, although blob regularization seems to exhibit a somehow irregular behaviors. It would be interesting to see whether these regularized models have similarities in the behavior of the complex singularities. In [13] it was in fact given evidence that the Euler-α regularization of the BR equation develops complex singularities, similarly to the results presented

here. The relevant approximation with viscous layers, not considered here, has a fundamental importance. For wall bounded flows there are results in different contexts (see e.g. [16, 54, 40] and references therein), and we postpone to [12] the analysis of the influence of the viscosity effects on the dynamics of layer of small thickness. It would be also interesting to study the behavior of the layer using the framework of the matched asymptotics as it is usually done for wall bounded flows, see e.g. [18, 19, 41] where it is suggested that analyticity might be necessary for the tangential variable only. An inner expansion technique for vortex layer was in fact used in [17] to derive an approximation of the flow inside the layer, see also [57] in a different context; matching with the outer flow is however more challenging with respect to the wall bounded flow counterpart, because the outer Euler flow is not a priori known due to the layer motion, although it might be necessary to achieve the justification of the BR model as a zero viscosity approximation of Navier–Stokes solutions.

ACKNOWLEDGMENTS. The work of the authors has been partially supported by GNFM of INdAM. The authors would like to thank an anonymous reviewer for comments and suggestions that helped improving the presentation of the paper.

REFERENCES

[1] D. H. BAILEY - J. M. BORWEIN - R. E. CRANDALL - I. J. ZUCKER, *Lattice sums arising from the Poisson equation*, J. Phys. A: Math. Theor. 46 (2013), no. 11, 115–201.

[2] G. R. BAKER - J. T. BEALE, *Vortex blob methods applied to interfacial motion*, J. Comp. Phys. 196 (2004), no. 1, 233–258.

[3] G. R. BAKER - D. I. MEIRON - S. A. ORSZAG, *Generalized vortex methods for free-surface flow problems*, J. Fluid Mech. 123 (1982), 477–501.

[4] G. R. BAKER - A. NACHBIN, *Stable methods for vortex sheet motion in the presence of surface tension*, SIAM J. Sci. Comp. 19 (1998), 1737–1736.

[5] G. R. BAKER - L. D. PHAM, *A comparison of blob methods for vortex sheet roll-up*, J. Fluid Mech. 547 (2006), 297–316.

[6] G. R. BAKER - M. J. SHELLEY, *On the connection between thin vortex layers and vortex sheets*, J. Fluid Mech. 215 (1990), 161–194.

[7] C. BARDOS - J. S. LINSHIZ - E. S. TITI, *Global regularity for a Birkhoff–Rott-α approximation of the dynamics of vortex sheets of the 2d Euler equations*, Physica D: Nonlinear Phenomena 237 (2008), no. 14–17, 1905–1911.

[8] D. BENEDETTO - C. MARCHIORO - M. PULVIRENTI, *The 2-D incompressible Euler flow for singular initial conditions*, Nonlinear variational problems and partial differential equations (Isola d'Elba, 1990), Pitman Res. Notes Math. Ser., vol. 320, Longman Sci. Tech., Harlow, 1995, pp. 57–74.

[9] D. BENEDETTO - M. PULVIRENTI, *From vortex layers to vortex sheets*, SIAM J. Appl. Math. 52 (1992), no. 4, 1041–1056.

[10] R. E. CAFLISCH, *Singularity formation for complex solutions of the 3D incompressible Euler equations*, Physica D 67 (1993), no. 1–3, 1–18.

[11] R. E. CAFLISCH - F. GARGANO - M. SAMMARTINO - V. SCIACCA, *Complex singularities and PDEs*, Rivista di Matematica della Universita di Parma 6 (2015), no. 1, 69–133.

[12] R. E. Caflisch - F. Gargano - M. Sammartino - V. Sciacca, *Complex singularity analysis of vortex layer flow*, in preparation (2017).

[13] R. E. Caflisch - F. Gargano - M. Sammartino - V. Sciacca, *Regularized Euler-α motion of an infinite array of vortex sheets*, Boll. Unione Mat. Ital. 10 (2017), 113–141, doi:10.1007/s40574-016-0097-6.

[14] R. E. Caflisch - O. F. Orellana, *Long time existence for a slightly perturbed vortex sheet*, Comm. Pure Appl. Math 39 (1986), 807–838.

[15] R. E. Caflisch - O. F. Orellana, *Singular solutions and ill-posedness for the evolution of vortex sheets*, SIAM J. Math. Anal. 20 (1989), no. 2, 293–307.

[16] R. E. Caflisch - M. Sammartino, *Navier-Stokes equations on an exterior circular domain: construction of the solution and the zero viscosity limit*, Comptes Rendus de l'Acadmie des Sciences – Series I – Mathematics 324 (1997), no. 8, 861–866.

[17] R. E. Caflisch - M. Sammartino, *Vortex layers in the small viscosity limit*, "WASCOM 2005" – 13th Conference on Waves and Stability in Continuous Media, World Sci. Publ., Hackensack, NJ, 2006, pp. 59–70.

[18] M. Cannone - M. C. Lombardo - M. Sammartino, *Existence and uniqueness for the Prandtl equations*, Comptes Rendus de l'Acadmie des Sciences – Series I – Mathematics 332 (2001), no. 3, 277–282.

[19] M. Cannone - M. C. Lombardo - M. Sammartino, *Well-posedness of Prandtl equations with non-compatible data*, Nonlinearity 26 (2013), no. 3, 3077–3100.

[20] M. J. Chen - L. K. Forbes, *Accurate methods for computing inviscid and viscous Kelvin–Helmholtz instability*, Journal of Computational Physics 230 (2011), no. 4, 1499–1515.

[21] C. Cichowlas - M. E. Brachet, *Evolution of complex singularities in Kida-Pelz and Taylor-Green inviscid flows*, Fluid Dyn. Res. 36 (2005), no. 4–6, 239–248.

[22] G. M. Coclite - F. Gargano - V. Sciacca, *Analytic solutions and singularity formation for the peakon b-family equations*, Acta Appl. Math. 122 (2012), 419–434.

[23] S. J. Cowley, *Computer extension and analytic continuation of Blasius' expansion for impulsively flow past a circular cylinder*, J. Fluid Mech. 135 (1983), 389–405.

[24] S. J. Cowley - G. R. Baker - S. Tanveer, *On the formation of Moore curvature singularities in vortex sheets*, J. Fluid Mech. 378 (1999), 233–267.

[25] G. Della Rocca - M. C. Lombardo - M. Sammartino - V. Sciacca, *Singularity tracking for Camassa–Holm and Prandtl's equations*, Appl. Numer. Math. 56 (2006), no. 8, 1108–1122.

[26] M. R. Dhanak, *Equation of motion of a diffusing vortex sheet*, J. Fluid Mech. 269 (1994), 265–281.

[27] J. Duchon - R. Robert, *Global vortex sheet solutions of Euler equations in the plane*, Journal of Differential Equations 73 (1988), no. 2, 215–224.

[28] U. Frisch - T. Matsumoto - J. Bec, *Singularities of Euler flow? Not out of the blue!*, J. Stat. Phys. 113 (2003), no. 5, 761–781.

[29] F. Gargano - G. Ponetti - M. Sammartino - V. Sciacca, *Complex singularities in KdV solutions*, Ricerche di Matematica 65 (2016), no. 2, 479–490.

[30] F. Gargano - M. Sammartino - V. Sciacca, *Singularity formation for Prandtl's equations*, Physica D: Nonlinear Phenomena 238 (2009), no. 19, 1975–1991.

[31] F. Gargano - M. Sammartino - V. Sciacca, *High Reynolds number Navier-Stokes solutions and boundary layer separation induced by a rectilinear vortex*, Computers & Fluids 52 (2011), 73–91.

[32] F. Gargano - M. Sammartino - V. Sciacca - K. W. Cassel, *Analysis of complex singularities in high-Reynolds-number Navier-Stokes solutions*, J. Fluid Mech. 747 (2014), 381–421.

[33] F. Gargano - M. Sammartino - V. Sciacca - K. W. Cassel, *Viscous-inviscid interactions in a boundary-layer flow induced by a vortex array*, Acta Appl. Math. 132 (2014), 295–305.

[34] D. D. Holm - M. Nitsche - V. Putkaradze, *Euler-alpha and vortex blob regularization of vortex filament and vortex sheet motion*, J. Fluid Mech. 555 (2006), 149–176.

[35] T. Y. Hou - J. S. Lowengrub - M. J. Shelley, *The long-time motion of vortex sheets with surface tension*, Physics of Fluids 9 (1997), no. 7, 1933–1954.

[36] C. Klein - K. Roidot, *Numerical study of shock formation in the dispersionless Kadomtsev-Petviashvili equation and dispersive regularizations*, Phys. D 265 (2013), 1–25.

[37] C. Klein - K. Roidot, *Numerical study of the semiclassical limit of the Davey-Stewartson II equations*, Nonlinearity 27 (2014), no. 9, 2177–2214.

[38] C. Klein - K. Roidot, *Numerical study of the long wavelength limit of the Toda lattice*, Nonlinearity 28 (2015), no. 8, 2993–3025.

[39] R. Krasny, *A study of singularity formation in a vortex sheet by the point-vortex approximation*, J. Fluid Mech. 167 (1986), 65–93.

[40] I. Kukavica - M. C. Lombardo - M. Sammartino, *Zero viscosity limit for analytic solutions of the primitive equations*, Arch. Ration. Mech. Anal. 222 (2016), no. 1, 15–45.

[41] I. Kukavica - V. Vicol, *On the local existence of analytic solutions to the Prandtl boundary layer equations*, Commun. Math. Sci. 11 (2013), 269–292.

[42] J. G. Liu - Z. Xin, *Convergence of vortex methods for weak solutions to the 2D Euler equations with vortex sheet data*, Comm. Pure Appl. Math 48 (1995), 611–628.

[43] M. C. Lopes Filho - J. Lowengrub - H. J. Nussenzveig Lopes - Y. Zheng, *Numerical evidence of nonuniqueness in the evolution of vortex sheets*, ESAIM: Math. Mod. and Num. Anal. 40 (2006), no. 2, 225–237.

[44] A. J. Majda - A. L. Bertozzi, *Vorticity and incompressible flow*, Cambridge Texts in Applied Mathematics, vol. 27, Cambridge University Press, Cambridge, 2002.

[45] C. Marchioro, *Euler evolution for singular initial data and vortex theory: a global solution*, Comm. Math. Phys. 116 (1988), no. 1, 45–55.

[46] T. Matsumoto - J. Bec - U. Frisch, *The analytic structure of 2D Euler flow at short times*, Fluid Dyn. Res. 36 (2005), no. 4–6, 221–237.

[47] D. W. Moore, *The equation of motion of a vortex layer of small thickness*, Studies in Appl. Math. 58 (1978), no. 2, 119–140.

[48] D. W. Moore, *The spontaneous appearance of a singularity in the shape of an evolving vortex sheet*, Proc. Roy. Soc. London Ser. A 365 (1979), no. 1720, 105–119.

[49] D. W. Moore, *Numerical and analytical aspects of Helmholtz instability*, Proceedings of the Sixteenth International Congress of Theoretical and Applied Mechanics, Lyngby, Denmark, 1985, pp. 263–274.

[50] W. Pauls - U. Frisch, *A Borel transform method for locating singularities of Taylor and Fourier series*, J. Stat. Phys. 127 (2007), no. 6, 1095–1119.

[51] W. Pauls - T. Matsumoto - U. Frisch - J. Bec, *Nature of complex singularities for the 2D Euler equation*, Physica D 219 (2006), no. 1, 40–59.

[52] D. I. Pullin, *Numerical studies of surface-tension effects in nonlinear Kelvin–Helmholtz and Rayleigh-Taylor instability*, J. Fluid Mech 119 (1982), 507–532.

[53] P. G. Saffman, *Vortex dynamics*, Cambridge University Press, 1993.

[54] M. Sammartino - R. E. Caflisch, *Zero viscosity limit for analytic solutions of the Navier-Stokes equation on a half-space. II. Construction of the Navier-Stokes solution*, Comm. Math. Phys. 192 (1998), no. 2, 463–491.

[55] M. J. Shelley, *A study of singularity formation in vortex-sheet motion by a spectrally accurate vortex method*, J. Fluid. Mech. 244 (1992), 493–526.

[56] S.-I. Sohn, *Singularity formation and nonlinear evolution of a viscous vortex sheet model*, Physics of Fluids 25 (2013), no. 1, 014106.

[57] F. Sueur, *Viscous profiles of vortex patches*, Journal of the Institute of Mathematics of Jussieu 14 (2015), no. 1, 1–68.

[58] C. Sulem - P.-L. Sulem - C. Bardos - U. Frisch, *Finite time analyticity for the two- and three-dimensional Kelvin–Helmholtz instability*, Comm. Math. Phys. 80 (1981), no. 4, 485–516.

[59] G. Tryggvason - W. J. A. Dahm - K. Sbeih, *Fine structure of vortex sheet rollup by viscous and inviscid simulation*, Journal of Fluids Engineering 113 (1991), no. 1, 31–36.

[60] J. A. C. Weideman, *Computing the dynamics of complex singularities of nonlinear PDEs*, SIAM J. Appl. Dyn. Syst. 2 (2003), no. 2, 171–186 (electronic).

[61] S. Wu, *Mathematical analysis of vortex sheets*, Comm. Pure Appl. Math. 59 (2006), no. 8, 1065–1206.

[62] X. Zhong, *Additive semi-implicit Runge–Kutta methods for computing high-speed non-equilibrium reactive flows*, J. Comp. Phys. 128 (1996), no. 1, 19–31.

Received 31 December 2016,
and in revised form 25 January 2017.

Francesco Gargano
Department of Energy, Engineering of
the Information and Mathematical Models
University of Palermo
Viale delle Scienze, Ed. 9
90128 Palermo, Italy
francesco.gargano@unipa.it

Marco Maria Luigi Sammartino
Department of Mathematics
University of Palermo
Via Archirafi 34
90123 Palermo, Italy
marcomarialuigi.sammartino@unipa.it

Vincenzo Sciacca
Department of Mathematics
University of Palermo
Via Archirafi 34
90123 Palermo, Italy
vincenzo.sciacca@unipa.it